

**${}^2\text{H}(\alpha, p\alpha)n$  reaction between 9.735 and 11.30 MeV**

S. S. Dasgupta,\* R. J. Slobodrian, R. Roy, C. Rioux, and F. Lahlou

*Université Laval, Département de Physique, Laboratoire de Physique Nucléaire, Québec G1K 7P4, Canada*

(Received 29 February 1980)

A kinematically complete experiment has been performed to study the deuteron breakup by  $\alpha$  particles at six incident energies between  $E_\alpha = 9.735$  and  $E_\alpha = 11.30$  MeV (3.245 to 3.77 MeV in c.m.), very close to threshold. The data show strong energy dependence. Final-state calculations with the  $\alpha p$  and  $\alpha n$  interactions provide only fair fits, but the addition of three-body forces produces a significant improvement.

$$\left[ \text{NUCLEAR REACTIONS } {}^2\text{H}(\alpha, p\alpha)n, E = 9.735 \text{ to } 11.30 \text{ MeV; measured} \right]$$

$$\sigma(E_p, \theta_p, \theta_\alpha): \text{ gas target.}$$

## I. INTRODUCTION

The alpha-neutron-proton system should be an obvious next step to the three nucleon system, for investigations of three-body problems. This particular system contains, to a good approximation, a structureless boson, and all particles are distinguishable.

Thus, recently, a significant amount of interest has been shown by a number of groups<sup>1-3</sup> to investigate, both theoretically and experimentally, the alpha-induced deuteron breakup. Experimental data from kinematically complete experiments, available so far, are at incident energies  $E_\alpha \geq 15$  MeV. At higher energies, the data seem to agree reasonably well with a modified impulse approximation<sup>7</sup> (henceforth abbreviated MIA), showing the importance of quasifree scattering. At the two lower energies ( $E_\alpha = 15$  and 18 MeV), such fits are less adequate and a Faddeev analysis using  $n\alpha$  and  $p\alpha$  interactions in the final state seems to provide better fits to the experimental data. Final-state interactions are likely to be dominant near the breakup threshold.

In the present work, we measured the energy dependence of the correlation cross sections of the  ${}^2\text{H}(\alpha, p\alpha)n$  reaction between 3.07 and 3.77 MeV center-of-mass energies, leading to very low kinetic energies for the three final-state bodies: 0.84 to 1.54 MeV.

## II. EXPERIMENTAL PROCEDURES

An  $\alpha$ -particle beam from the Université Laval 7.5 MV Van de Graaff accelerator was incident on deuterium contained in a 53 cm diameter scattering chamber. The scattering chamber was isolated by 2.1 mg  $\text{cm}^{-2}$  Havar foils from the accelerator tube and the Faraday cup. The beam spot was less than 2 mm in diameter. The energy of the incident beam was varied from 10.50 and 12.00 MeV. Due

to energy loss of  $\alpha$  particles in the Havar foil and deuterium gas, the energy at the center of the target varied between 9.735 and 11.30 MeV. Five energy steps in this energy range were used.

The particles were detected with two surface barrier detectors mounted behind collimators with rectangular slits of width 0.35 cm, back slit height 0.45 cm, and interslit distance 14.0 cm. The resulting geometry factor is  $G = 1.72 \times 10^{-4} \text{ sr}^2 \text{ cm}$  and the angular resolution is  $\pm 1.1^\circ$ . The detectors were placed at angles  $15^\circ(\theta_\alpha)$  and  $-30^\circ(\theta_p)$  for all energies. The  $\alpha$ -particle angle selected was close to the kinematical maximum for the lowest energy. Thus there was no possibility of reverse correlation, i.e.,  $\alpha$ 's in the  $-30^\circ$  detector and protons in the  $15^\circ$  detector. A schematic diagram of the gas scattering geometry used in this experiment is shown in Fig. 1.

A block diagram of the electronics and the data acquisition system is shown in Fig. 2. This sys-

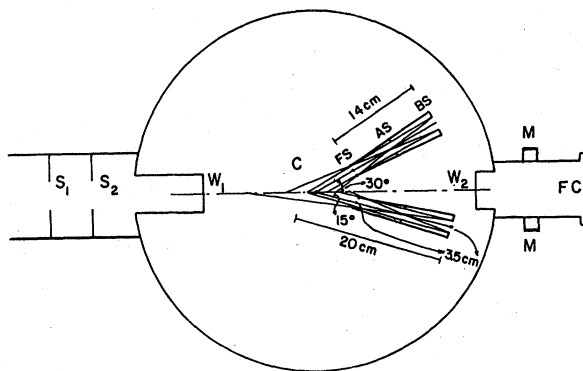


FIG. 1. Schematic view of the scattering chamber and of the collimators.  $S_1, S_2$ : defining slits;  $W_1, W_2$ : Havar windows; C: center of rotation of the detectors; FS: vertical front slit; AS: antiscattering aperture; BS: rectangular back aperture; FC: Faraday cup; and M: secondary-electron-trapping magnet.

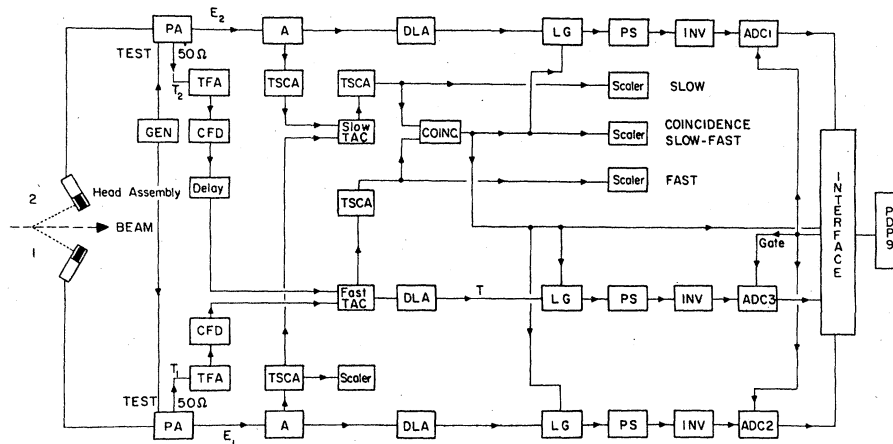


FIG. 2. Block diagram of the electronics. GEN: pulse generator; PA: pre-amplifier; TFA: timing filter amplifier; CFD: constant fraction timing discriminator; A: amplifier; TSCA: timing single channel analyzer; TAC: time-to-amplitude converter; COINC: coincidence unit; DLA: delay line amplifier; LG: linear gate; PS: pulse stretcher; INV: inverter; and ADC: analog-to-digital converter.

tem is described in detail elsewhere.<sup>9</sup> In brief, a fast-slow coincidence technique was used. Several changes had to be made. Hydrogen (and deuterium) passivated detectors were used and, due to large energy loss by  $\alpha$  particles, the nickel foils were taken off. The thresholds in the fast side had to be lowered to 250 keV. Three signals were produced by the electronics, two proportional to the energies  $E_1$  and  $E_2$ , one proportional to the difference of the times of arrival  $T = T_2 - T_1$ . Due to the large difference between proton and alpha times of flight along the kinematic locus, particularly for low energy alphas, the time spectrum resolution was considerably reduced as the prompt peak was smeared. Thus a correction was necessary and this was done by a computer program which calculated and corrected the time of flight, event by event, from the  $E_1 - E_2$  values. A typical time spectrum before and after such a correction is shown in Fig. 3.

To normalize the breakup data at the end of each run, the detectors were set at elastic  $\alpha$ - $d$  correlation angles and the yield noted for a fixed incident beam charge, monitored by the Faraday cup. The spectra obtained in such runs were also used for calibration of  $E_1$ ,  $E_2$ , and time-to-amplitude converters (TAC).

### III. DATA ANALYSIS

The  $E_1$  vs  $E_2$  bidimensional spectra were obtained for a digital gate on the corrected prompt time peak spectrum. Figure 4 shows one such plot with the kinematic band superimposed on it. The central kinematic line is for the nominal angles, whereas the other two are for the corre-

sponding angular limits determined by the geometry. The calculated kinematic band agrees well with experiment at all energies under investigation. The number of events outside the region of the kinematic band was generally low compared to that inside the band. The number of random coincidences was obtained from an  $E_1$  vs  $E_2$  plot using a digital gate on regions outside the peak of the time spectrum.

The numbers in the band were projected along the central arc, and convenient bites (250 keV)

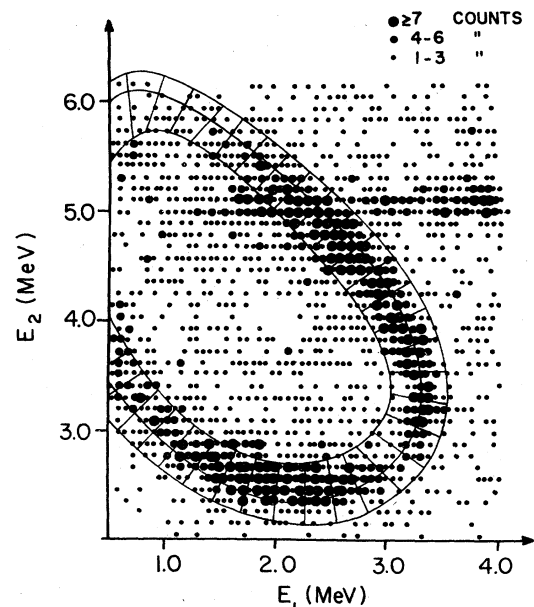


FIG. 3. Kinematic arcs with bites on arc length superimposed on an experimental data plot, for 11.3 MeV.

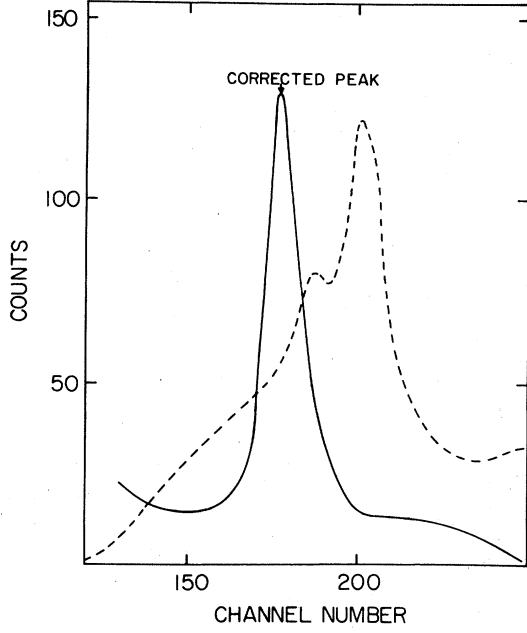


FIG. 4. Time spectrum before and after correction. Time scale: 8 ch/nsec.

of these arc projected numbers were transformed into correlation cross sections  $d^3\sigma/d\Omega_\alpha d\Omega_p ds$ , with the proper  $G$  factors. The data were normalized to the elastic  $\alpha$ - $d$  scattering cross sections of Ohlsen and Young.<sup>10</sup>

Errors are due mainly to the statistics of the number of counts. Cross sections are shown in Table I. Table II shows total breakup cross sections  $d^2\sigma/d\Omega_\alpha d\Omega_p$  vs energy.

#### IV. THEORY

The three particles are labeled as follows:  $\alpha$ -1, proton-2, and neutron-3. The breakup cross section is given by

$$\frac{d^3\sigma}{d\Omega_1 d\Omega_2 dE_1} = K\rho |T_{fi}|^2, \quad (1)$$

where  $K$  is a constant,  $\rho$  is the phase space factor given by<sup>11</sup>

$$\rho \cong h^{-6} m_N m_1 p_{12}^2 (2 + \cos\theta_{12})^{-1}, \quad (2)$$

where  $m_N$  is the average nucleon mass,  $h$  is Planck's constant, and  $\cos\theta_{12} = \cos\theta_1 \cos\theta_2 + \sin\theta_1 \sin\theta_2 \cos\phi_{12}$ ;  $T_{fi}$ , the  $T$  matrix, can be written as<sup>12</sup>

$$\begin{aligned} T_{fi} &= T_{12} + T_{13} + T_{23} + T_{12}G_0T_{13} + T_{12}G_0T_{23} \\ &+ \dots \text{higher order terms} \\ &\approx T_{12} + T_{13}. \end{aligned} \quad (3)$$

For these two-body terms the effective range approximation in final-state interaction theory<sup>13</sup> is for  $n$ - $\alpha$

$$\begin{aligned} |T|^2 &\approx \frac{\sin^2\delta_l}{k^{2l}} = \frac{k^{2l+2}}{k^{4l+2} \cot^2\delta_l + k^{4l+2}} \\ &= \frac{1}{k^{2l} \cot^2\delta_l + k^{2l}}, \end{aligned} \quad (4)$$

$k^l \cot\delta_l = 1/a + \frac{1}{2}rk^2$ , and corresponding Coulomb formulas for  $p$ - $\alpha$ ,<sup>14</sup> where  $a$  and  $r$  are the scattering length and effective range, respectively. For our calculations we use the effective range parameters of Arndt *et al.*<sup>15</sup>

#### V. RESULTS AND DISCUSSION

The triple correlation cross sections vs arc are plotted in Fig. 5 along with the effective range

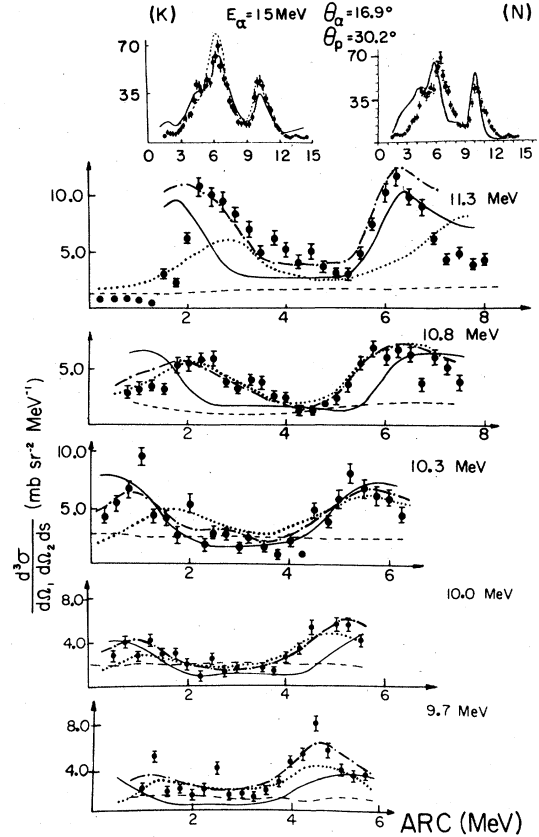


FIG. 5.  $(d^3\Omega)/(d_1 d \Omega_2 ds)$  vs arc length. Solid curves show sum of  $\alpha p$  and  $n\alpha$  cross sections. Rounded off energies are indicated. The broken lines are corresponding phase space distributions. The calculations referred to in the Note added are indicated by dotted lines. The dash dot lines are least squares fits to the data with the incoherent addition of solid and dotted line contributions. Inserts: data at 15 MeV and  $\theta_\alpha = 16.9^\circ$ ,  $\theta_p = 30.2^\circ$  (Ref. 5) together with MIA and Faddeev calculations; --- MIA calculations; (K) from Ref. 7 and (N) from Ref. 8.

TABLE I.  $d^3\sigma/d\Omega_1 d\Omega_2 ds$  vs arc length ( $\text{mb sr}^{-2} \text{MeV}^{-1}$ ).

$E_{\text{arc}}(s)$ (MeV)	9.735 MeV	10.00 MeV	10.27 MeV	10.79 MeV	11.3 MeV
0.25	4.54±0.51	2.92±0.51	4.09±0.66	2.99±0.55	1.02±0.29
0.50	2.36±0.37	4.10±0.61	5.27±0.75	3.30±0.58	1.02±0.29
0.75	5.18±0.55	2.73±0.50	6.56±0.84	3.71±0.62	1.02±0.29
1.00	2.13±0.35	4.28±0.63	9.68±1.02	3.29±0.58	0.71±0.26
1.25	2.36±0.36	2.92±0.52	4.19±0.67	5.66±0.76	0.42±0.19
1.50	1.73±0.32	3.00±0.52	3.77±0.64	5.87±0.78	3.40±0.54
1.75	2.30±0.36	2.00±0.43	2.47±0.52	6.08±0.79	2.55±0.47
2.00	4.20±0.49	0.91±0.29	5.38±0.76	6.18±0.80	6.73±0.76
2.25	1.78±0.32	2.46±0.47	1.51±0.40	4.02±0.64	11.41±0.98
2.50	1.90±0.33	1.37±0.35	2.69±0.54	3.40±0.59	10.73±0.96
2.75	1.55±0.30	1.55±0.38	2.47±0.52	4.22±0.66	9.97±0.92
3.00	2.18±0.35	0.27±0.16	1.18±0.36	3.91±0.63	8.70±0.86
3.25	2.87±0.41	1.73±0.40	2.15±0.48	2.78±0.53	7.32±0.79
3.50	4.83±0.53	1.31±0.35	1.29±0.37	2.58±0.51	5.02±0.65
3.75	5.52±0.56	2.82±0.51	0.75±0.29	1.24±0.36	6.47±0.74
4.00	8.22±0.69	3.46±0.56	1.94±0.46	1.24±0.36	5.28±0.67
4.25	4.92±0.58	5.37±0.70	0.75±0.29	1.96±0.45	4.17±0.60
4.50	4.14±0.49	7.93±0.85	4.84±0.72	2.37±0.49	5.20±0.67
4.75	3.82±0.46	5.83±0.73	3.77±0.64	3.91±0.63	3.83±0.37
5.00	3.80±0.47	5.83±0.73	5.92±0.80	5.87±0.78	3.15±0.52
5.25	2.13±0.35	4.28±0.62	6.28±0.94	7.20±0.86	3.00±0.50
5.50			6.99±0.87	6.28±0.80	4.85±0.64
5.75			6.46±0.83	7.00±0.85	7.60±0.80
6.00			6.03±0.81	6.69±0.83	10.65±0.95
6.25			4.73±0.71	3.71±0.62	12.20±1.02
6.50				6.39±0.81	10.05±0.93
6.75				5.36±0.74	9.11±0.88
7.00				3.91±0.63	6.13±0.72
7.25					4.26±0.60
7.50					4.70±0.63
7.75					3.66±0.56
8.00					4.09±0.59

calculations for  $\alpha p$  and  $\alpha n$  interactions. An insert shows similar results from Koersner<sup>5</sup> at 15 MeV and angles 16.9° and 30.2°, close to ours, with Faddeev calculations through sequential decay of  ${}^6\text{Li}$  by Koike<sup>7</sup> and MIA calculations by Nakamura.<sup>8</sup> Our data at lower energies and calculations show fits quite comparable to theirs. This suggests the following two points: First, the final state interactions  $\alpha p$  and  $\alpha n$  are predominant in the  $\alpha d$

TABLE II.  $d^2\sigma/d\Omega_\alpha d\Omega_p$  (integrated breakup cross section) vs energy.

$E_\alpha$ (MeV)	$\frac{d^2\sigma}{d\Omega_\alpha d\Omega_p}$ (mb/sr <sup>2</sup> )
9.735	73.2±2.0
10.000	67.1±2.4
10.270	103.2±3.3
10.790	121.0±3.5
11.300	178.5±3.9

breakup correlation at our energies. Second, the fact that a calculation considering a sequential decay through the formation of  ${}^6\text{Li}$  fits equally well, shows the lack of importance of the sequential decay process through levels of  ${}^6\text{Li}$  with respect to the *shape* of the correlation spectra. At the lowest energy (9.735 MeV) the fit is significantly worse. A missing ingredient in all the theoretical treatments and calculations, thus far, is the consideration of three body forces. They may become more important at energies close to the three body breakup threshold, for simple kinematic reasons, and may explain the deterioration of fits based on two-body forces only.

It is kinematically impossible at our energies to populate the  $1^+$  and  $3^+$  levels of  ${}^6\text{Li}$ ,<sup>16</sup> as considered by Koike.<sup>7</sup> However, a  $(J^\pi, T)$  ( $2^+, 0$ ) state of  ${}^6\text{Li}$  may be involved. A sequential decay through  ${}^6\text{Li}$  at our energies should proceed through the broad  $J^\pi=2^+$  state of  ${}^6\text{Li}$  at 4.7 MeV.<sup>17</sup> Figure 6 shows fairly conclusively that such is the case, as the breakup correlation excitation function follows

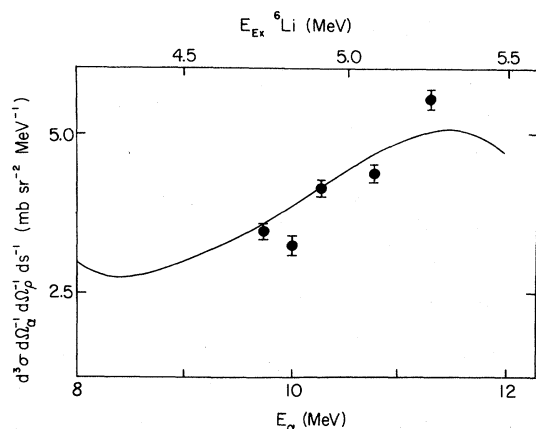


FIG. 6. Excitation function of the average cross section per unit arc for the breakup correlation. The solid line is a plot of the excitation function of the  $\alpha$ - $d$  elastic  $90^\circ$  cross section showing the effect of the 4.7 MeV state in  ${}^6\text{Li}$ , mentioned in the text, and indicating that the breakup correlation closely follows this trend.

closely that of the elastic  $\alpha$ - $d$  cross section.

Further developments in the theoretical treatment, including exactly Coulomb effects (and three body forces if possible), are clearly necessary in view of the limited success in all attempts to fit the alpha-induced deuteron breakup correlations at low energies.

*Note added:* It has been noticed recently<sup>18</sup> that in the  $p+d \rightarrow p+p+n$  reaction very near threshold there is an excellent agreement of the experimental correlations with calculations based on the two-pion exchange three-body forces,<sup>19</sup> producing in lowest order a transition probability proportional to  $p_{2,3} \cdot p_{1,3}$ , product of the relative momenta of particles 2-3 and 1-3 (3=neutron). A similar approach in the present case has produced a remarkable improvement of the calculated curves with experiment at 10.27, 10.79, and 11.3 MeV.<sup>20</sup> We show in Fig. 5 such calculations for those energies and also for 9.735 and 10.00 MeV reported here. It is apparent that the three-body correlation based on three-body forces dominates the experimental results at the lowest energies. A least squares fit to the data with two- and three-body force contributions is also shown in Fig. 5. The fraction of the latter is, from 11.3 MeV down, 0.48, 0.63, 0.50, 0.51, and 0.54. Koike<sup>21</sup> has just performed Faddeev calculations using two body forces, including Coulomb corrections, corresponding to our data at 11.3 MeV. The theoretical cross section had to be renormalized by a factor 0.25 to bring it to the level of experiment (at higher energies the factor was 0.5). Qualitative agreement is found after renormalization over a limited region of the spectrum, with an average chi-squared per point  $\langle \chi_p^2 \rangle = 11.45$ . Over the same region, with two- and three-body forces we have obtained  $\langle \chi_p^2 \rangle = 1.7$ .

\*Present address: The University of Burdwan, Burdwan 713 101, India.

<sup>1</sup>T. Rausch, H. Zell, D. Wallenwein, and W. Von Witsch, Nucl. Phys. **A222**, 429 (1974).

<sup>2</sup>K. Prescher, W. Bretfeld, W. Burgmer, H. Eichner, H. J. Helten, H. Klein, H. Kretzner, H. Stehl, and W. W. Wohlfarth, Nucl. Phys. **A286**, 142 (1977).

<sup>3</sup>E. Hourany, H. Nakamura, F. Takeitchi, and T. Yuasa, Nucl. Phys. **A222**, 537 (1974).

<sup>4</sup>K. Sagara, T. Motobayashi, N. Takahashi, Y. Hashimoto, M. Hara, Y. Nogami, H. Noya, and H. Nakamura, Nucl. Phys. **A273**, 493 (1976).

<sup>5</sup>I. Koersner, L. Glantz, A. Johansson, B. Sundquist, H. Nakamura, and H. Noya, Nucl. Phys. **A286**, 431 (1977).

<sup>6</sup>K. Sagara, T. Motobayashi, N. Takahashi, T. Hashimoto, M. Hara, U. Nogami, H. Nakamura, and H. Noya, Nucl. Phys. **A299**, 77 (1978).

<sup>7</sup>Yasuro Koike, Nucl. Phys. **A301**, 411 (1978).

<sup>8</sup>H. Nakamura, Nucl. Phys. **A208**, 207 (1973).

<sup>9</sup>B. Frois, J. Birchall, C. R. Lamontagne, U. von Moellendorff, R. Roy, and R. J. Slobodrian, Phys. Rev. C **8**, 2132 (1973).

<sup>10</sup>G. G. Ohlsen and P. G. Young, Nucl. Phys. **52**, 134 (1964).

<sup>11</sup>G. G. Ohlsen, Nucl. Instrum. Methods **37**, 240 (1965).

<sup>12</sup>G. D. Thijs, P. H. Schram, and C. C. Jonker, Nucl. Phys. **A205**, 413 (1973).

<sup>13</sup>K. M. Watson, Phys. Rev. **88**, 1163 (1952).

<sup>14</sup>R. J. Slobodrian, Rep. Prog. Phys. **34**, 175 (1971) and references therein.

<sup>15</sup>Richard A. Arndt and L. David Roper, Nucl. Phys. **A209**, 447 (1973).

<sup>16</sup>F. Ajzenberg Selove, Nucl. Phys. **A227**, 1 (1974); **78**, 1 (1966).

<sup>17</sup>W. Gruebler, P. A. Schmelzbach, V. König, R. Risler, and D. Boerma, Nucl. Phys. **A242**, 265 (1975).

<sup>18</sup>R. J. Slobodrian, S. S. Dasgupta, C. Rioux, F. Lahlou, and R. Roy (unpublished).

<sup>19</sup>B. H. J. McKellar, in *Few Body Dynamics*, edited by A. N. Mitra, I. Slaus, V. S. Bhasin, and V. K. Gupta (North-Holland, Amsterdam, 1976), p. 508 and references therein.

<sup>20</sup>S. S. Dasgupta, R. Roy, C. Rioux, F. Lahlou, and R. J. Slobodrian, Phys. Lett. **91B**, 32 (1980).

<sup>21</sup>Y. Koike (private communication and unpublished).